J. Electrochem. Sci. Eng. **14(3)** (2024) 339-352; http://dx.doi.org/10.5599/jese.2036

Open Access : : ISSN 1847-9286
https://pub.iapchem.org/ojs/index.php/JESE

Original scientific paper

Development of electrode by using gold-platinum alloy nanoparticles for electrochemical detection of serum amyloid A protein

Kalpana Ladi and Aditya Sharma Ghrera✉

The NorthCap University, Applied Science Department, Gurugram, Haryana, India, 122017

Corresponding author: ✉adityasghrera@gmail.com

Received: August 23, 2023; Accepted: February 11, 2024; Published: April 29, 2024

Abstract

Gold-platinum alloy nanoparticles (AuPtNP) were electrochemically deposited on the surface of indium-tin-oxide (ITO) modified with (3-aminopropyl)triethoxysilane (APTES), after optimizing deposition conditions for the electroplating solution and number of deposition cycles. Different part ratios of Au/Pt used were 4/0, 3/1, 2/2, 1/3 and 0/4 (AuNP, Au_3Pt_1, Au_2Pt_2, Au_1Pt_3 and PtNP, respectively) in preparation of 1 mM solutions. FE-SEM, EDAX and XRD surface characterization techniques were used to confirm the presence of deposited AuPt alloy nanoparticles on the modified ITO surface. Electrochemical methods (CV, DPV and EIS) were used to investigate the electrochemical properties of prepared electrodes in the presence of ferri/ferrocyanide redox couple, which indicated the following increasing order of electrocatalytic peak current: Au < Au_2Pt_2 < Pt < Au_1Pt_3 < Au_3Pt_1. The most active electrode, Au_3Pt_1NP/APTES/ITO (with Au/Pt part ratio 3:1), was further used to fabricate the immunoelectrode SAA-Ab/Au_3Pt_1NP/APTES/ITO. The prepared immunoelectrode was tested for detection of serum amyloid A protein biomarker (APO-SAA) by immobilising SAA-specific antibodies (SAA ½ Ab) on its surface. Sensing studies on this immunoelectrode, performed by DPV technique, revealed the SAA biomarker detection in the linear range of 10 to 10^6 fg ml^{-1}. The limit of detection was calculated as 7.0 fg ml^{-1}.

Keywords

Electrochemical biosensing; bimetallic nanoparticles; electrocatalysts; immunoelectrode; inflammatory biomarker

Introduction

Bimetallic nanoparticles have gained great attention due to their unique catalytic efficiency, low cost, high stability, high electronic and optical properties. The presence of the second metal affects many parameters of prepared alloys like particle size, composition alterations, shape, surface morphologies, chemical and physical properties of materials, including catalytic activities and selectivity. Bimetallic nanoparticles of platinum and gold have proven their extraordinary electrocatalytic properties and are used for various applications, including fuel cells and biosensing [1-4].

Pt with outstanding electrocatalytic properties and Au with more electronegativity and less reactivity produce synergistic catalytic effects due to their interaction in their alloy [5-7]. The greater availability of gold at a lower price than platinum favors this combination of metal nanoparticles to tap the benefits of both in one alloy besides reducing the cost of preparation of electrode [8-11]. Electrochemical deposition of Au-Pt nanoparticles is a simple, easy, and direct method to fabricate electrodes with AuPtNP alloy film.

Indium tin oxide (ITO) has a wide range of applications and can be used in fields such as biosensors, transistors, electroluminescence devices, light-emitting diodes, solar cells and displays. Its surface can be modified in different ways to enhance its electrocatalytic activity [5,12,13]. Due to high transparency, excellent electrical conductivity and large conducting surface area, ITO has wide potential to be used as a working electrode for electrochemical deposition of AuPtNP alloy film. As it can be easily etched and patterned, electrochemical biosensors can be fabricated using modified ITO surfaces to detect various biomolecules of interest [12].

Serum amyloid A (SAA) protein, an inflammatory biomarker, has recently gained attention as its concentration in human serum increases manifolds immediately after viral infection in the human body, which helps in the early detection of viral diseases. Its concentration may increase many times its original concentration and decrease at a faster rate during recovery from the infection [14-16]. Fabricating an electrochemical biosensor to detect biomarkers is easy, cost-effective, less time-consuming, and non-invasive as compared with the other techniques to detect SAA biomarker. These biosensors are sensitive, reproducible, reliable, selective, and stable towards target biomolecules and hence possess wide potential in clinical diagnosis [17,18].

Xia *et al.* reported SAA electrochemical immunoassay [19] to detect SAA as a chronic inflammatory biomarker, while Lee *et al*. reported the fabrication of anodic aluminum oxide (AAO) chip for the detection of SAA 1 as a lung cancer biomarker [20]. Antibody array-based immunosensor was developed by Timucin *et al*. [21] to detect SAA as a cardiovascular disease biomarker, [11,22] presented the detection of SAA as a renal cell carcinoma biomarker in their report. SAA as an inflammatory rheumatic disease biomarker and for allograft rejection was reported by Sorić Hosman *et al.* [23], while SAA as a prominent acute phase reactant biomarker was reported by Malle *et al*. [16].

In the present manuscript, electrochemical deposition condition parameters were firstly optimized for the alloy of gold-platinum nanoparticles (AuPtNP) on the ITO surface. AuPtNP hybrids were electrochemically deposited on the ITO surface with different part ratios of Au and Pt salts in the electrolyte. Electrode with part ratio 3:1 for Au and Pt, respectively (Au_3Pt_1NP) was found to be of greater electrocatalytic activity and was further used to detect SAA biomarker by immobilizing antibodies on the surface of the optimized electrode (Scheme 1).

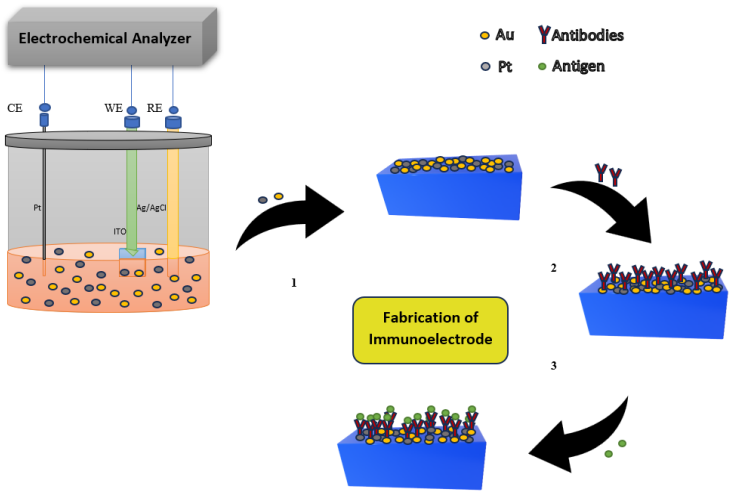

Scheme 1. *Scheme for fabrication of SAA-Ab/AuPtNP/APTES/ITO immunoelectrode*

The procedures for modification of ITO surface with APTES, preparation of electrolytic solutions and antibody immobilization have already been reported in our previous works [24,25].

Experimental

Chemicals and reagents

Hexachloroplatinic acid hexahydrate ($H_2PtCl_6{\cdot}6H_2O$) was purchased from SRL (Sisco Research Laboratories) and hydrogen tetrachloroaurate(III) ($HAuCl_4{\cdot}3H_2O$) was purchased from CDH. (3-aminopropyl)triethoxysilane (APTES) (Himedia make), SAA $^1/_2$ antibodies (Affinity Biosciences), and Prospec make serum amyloid A protein (APO-SAA) were used. Solution of 100 mM PBS (pH 7.4) containing 5 mM $[Fe(CN)6]^{3-/4-}$ was prepared by using 0.2 M sodium phosphate dibasic dihydrate ($Na_2HPO_4{\cdot}2H_2O$) and 0.2M sodium phosphate monobasic dihydrate ($NaH_2PO_4{\cdot}2H_2O$) on 100 ml ultrapure water along with adding 0.9 % NaCl. For 5 mM $[Fe(CN)6]^{3-/4-}$, 0.211 g of potassium ferrocyanide and 0.165 g of potassium ferricyanide were added to the 100 ml PBS solution prepared. Other chemicals were supplied and prepared, as reported previously [24,25].

Instrumentation

For electrochemical deposition and characterization, an advanced Metrohm potentiostat/galvanostat 204 was used with a three-electrode system [24,25] containing Ag/AgCl/3 M KCl reference electrode and Pt wire as a counter electrode. Electrochemical characterization techniques used were cyclic voltammetry (CV), electrochemical impedance spectroscopy (EIS) and differential pulse voltammetry (DPV) in 100 mM PBS buffer solution with 0.9 % NaCl and 5 mM $[Fe(CN)_6]^{3-/4-}$ (pH 7.4). EIS measurements were performed using alternating signal amplitude of 10 mV, dc potential of 0.03 V and frequency range of 10^5 to 0.1 Hz.

For morphological characterization of AuPtNP-modified electrodes, FE-SEM (JEOL JSM-7610F Plus with attached EDX analysis tool) was Shimadzu UV2600sed. A 20 kV operation voltage was used over a collection period of 164 seconds to obtain the EDX spectrum. To determine the crystalline structures of the deposits, an X-ray diffraction (XRD) analyzer (Rigaku SmartLab StudioII, λ = 0.1541 nm, Cu Kα radiation) was used. UV measurements were performed by Shimadzu UV2600 spectrophotometer.

Optimization of electrochemical deposition parameters for AuPtNP deposition on ITO surface

AuPtNP were deposited electrochemically from two different solutions (labelled as solution A and B, both containing platinum salts $H_2PtCl_6{\cdot}6H_2O$ and $HAuCl_4{\cdot}3H_2O$) on the surface of ITO with and without its modification with APTES. The CV technique was applied in the potential range of -0.6 to 1.0 V and a scan rate of 100 mV s^{-1} for 20 cycles. Only slight changes were observed in redox peak currents after depositing AuPtNP for more than 60 cycles on the electrode surface.

AuPtNP were first deposited on ITO surface (with/without modification with APTES) from solution A (0.01 M Na_2SO_4, 0.01 M H_2SO_4 and 1 mM total concentration of $H_2PtCl_6{\cdot}6H_2O$ and $HAuCl_4{\cdot}3H_2O$), and then from solution B (0.05 M PBS (pH 7.0) and 1 mM total concentration of $H_2PtCl_6{\cdot}6H_2O$ and $HAuCl_4{\cdot}3H_2O$) [26]. The procedure for cleaning and modification of bare ITO electrodes of size 1×1 cm^2 with APTES was reported in previous works [24,25], along with a procedure for solution condition optimization.

Fabrication of different AuPtNP/APTES/ITO electrodes

To optimize Au and Pt metal salt proportion in deposition solution, AuPt nanoparticles were electrochemically deposited for 60 cycles on APTES/ITO electrodes from solution A containing noble metal salts of Au/Pt in different part ratios of 4:0, 3:1, 2:2, 1:3 and 0:4, respectively (with their total

molar concentration in deposition solution taken as 1mM) (Table 1). The corresponding electrodes are denoted as AuNP/APTES/ITO, Au_3Pt_1NP/APTES/ITO, Au_2Pt_2NP/APTES/ITO, Au_1Pt_3NP/APTES/ITO and PtNP/APTES/ITO, respectively.

Table 1. *Detailed information about the Au and Pt salts concentrations used for the deposition of AuPTNP on APTES/ITO electrodes*

Terminology adopted	Part of actual concentration of metallic salt (out of 1 mM concentration) in the electrolyte solution (Au salt + Pt salt)	Concentrations of metallic salts in 20 ml solution (Au salt + Pt salt), mM	Molar ratio of salts in solution
4:0	4:0	1.0 + 0.0	1:0
0:4	0:4	0.0 + 1.0	0:1
2:2	2:2	0.5 + 0.5	1:1
3:1	3:1	0.75 + 0.25	3:1
1:3	1:3	0.25 + 0.75	1:3

Results and discussion

Electrochemical characterization of variously deposited AuPtNP on ITO and APTES/ITO electrodes

AuPtNP (Au_2Pt_2) deposited for 20 cycles on bare ITO and APTES/ITO electrodes from solutions A and B were characterized by CVs recorded at 50 mV/s scan rate within -0.5 to 1.0 V potential range in 100 mM PBS buffer solution containing 5 mM $[Fe(CN)_6]^{3-/4-}$ (Figure 1a). The highest redox peak current was obtained for the AuPtNP/APTES/ITO electrode when AuPt nanoparticles were deposited from solution A. The reason for this could be easier electrochemical deposition in acidic conditions containing H_2SO_4.

Characterization of bare ITO and APTES/ITO modified with Au, Pt and AuPt metal nanoparticles was performed using CVs (at 50 mV/s scan rate and -0.6 V to 1.5 V potential range) in 0.05 M H_2SO_4 (Figure 1b) for electrodes AuNP/APTES/ITO, Au_2Pt_2NP/APTES/ITO and PtNP/APTES/ITO. The reduction peaks were observed at potentials 0.61 and 0.02 V for electrodes AuNP/APTES/ITO and PtNP/APTES/ITO, respectively. For electrode AuPtNP/APTES/ITO, two reduction peaks were observed at potentials 0.57 V and 0.07 V, corresponding to deposited AuNP and PtNP. These two peaks confirm the deposition of two noble metal alloy nanoparticles on ITO [27].

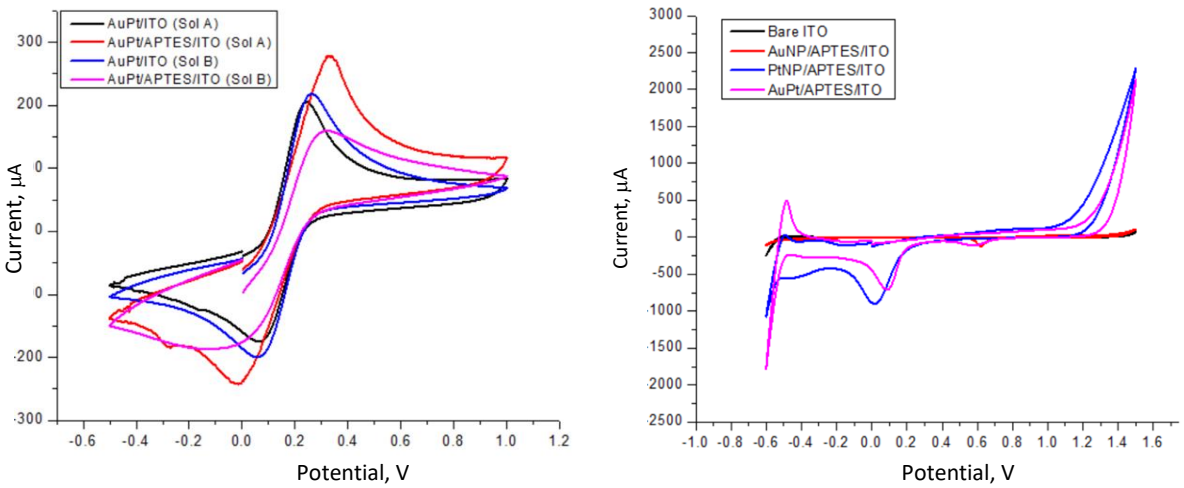

Figure 1. *CVs (50 mV s^{-1}) of: (a) AuPtNP (Au_2Pt_2) on ITO (with/without APTES on ITO surface) electrochemically deposited from solutions A and B for 20 cycles, recorded in 100 mM PBS, pH 7.4 containing 5 mM $[Fe(CN)_6]^{3-/4-}$; (b) bare ITO, AuNP/APTES/ITO, PtNP/APTES/ITO and AuPtNP/APTES/ITO recorded in 0.05 M H_2SO_4 (AuNP, PtNP, AuPtNP deposited for 20 cycles from solution A on APTES/ITO)*

Since the highest oxidation and reduction peak currents due to ferricyanide/ferrocyanide redox reaction were obtained for the APTES-modified ITO with AuPtNP deposited from solution A, solution A has been used throughout this study for deposition of AuPtNP.

FE-SEM and EDX (including elemental X-ray mapping) of deposited AuPt nanoparticles

FE-SEM surface morphological studies were conducted for Au_2Pt_2NP/APTES/ITO, Au_1Pt_3NP/ /APTES/ITO and Au_3Pt_1NP/APTES/ITO electrodes [1]. Electrodes with deposition of alloys of metal nanoparticles, Au_2Pt_2NP/APTES/ITO (Figure 2a), Au_1Pt_3NP/APTES/ITO (Figure 2b) and Au_3Pt_1NP/ /APTES/ITO (Figure 2c) electrodes, show cauliflower-like nanoparticles with numerous grains conglomeration which undergoes three step growth process of nuclei formation, aggregation of tiny particles on nuclei and then growth into crystal grains.

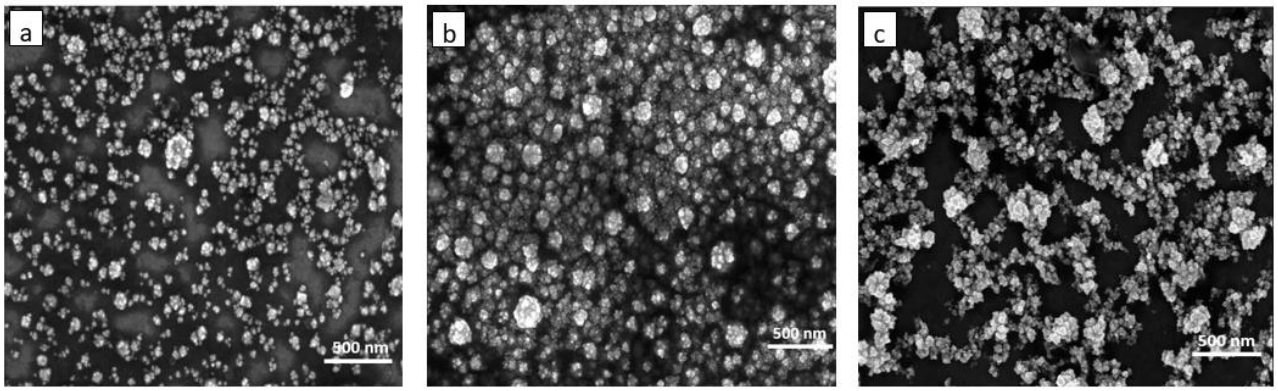

Figure 2. *FE-SEM images of: (a) Au_2Pt_2NP/APTES/ITO, (b) Au_1Pt_3NP/APTES/ITO, (c) Au_3Pt_1NP/APTES/ITO electrodes*

EDX analysis (along with elemental X-ray mapping) was also performed for all alloy deposited nanoparticles (Au_2Pt_2NP/APTES/ITO, Au_1Pt_3NP/APTES/ITO and Au_3Pt_1NP/APTES/ITO) which provided a more detailed elemental composition of these electrodes (Figure 3).

EDX results for various AuPtNP hybrids deposited on APTES/ITO confirm the presence of deposited Au and Pt on the electrode surfaces. Further, the varying content of Au and Pt in different hybrids follows their varying composition in the salt solution. EDX of the electrode with an electrochemically deposited film of Au_3Pt_1NP shows a higher content of Au as compared to Pt, whereas EDX of Au_1Pt_3NP electrode shows less elemental presence of Au as compared to Pt. It is worth noting that in the case of the Au_2Pt_2NP electrode, where the same molar concentrations of Au and Pt in the salt solution were used, the EDX presents a content of Pt as compared to Au. This may be because Pt tends to get deposited on the electrode surface better than Au. The increased tendency of PtNP deposition compared to AuNP deposition is also reflected for Au_1Pt_3 and Au_3Pt_1 electrodes, where the content is not directly correlated with the parts of their respective salts in the solution. Rather, the weight of PtNP deposited is higher compared to its part ratio in the salt solution.

XRD analysis of deposited AuPt metal nanoparticles

X-ray diffraction spectra of different AuPtNP/APTES/ITO electrodes are presented in Figure 4.

XRD diffraction patterns acquired for all prepared electrodes show different peaks, as listed in Table 2. In the 2θ range of 10 to 80°, different distinctive peaks have been obtained with (111), (200), (220) and (311) as their crystallographic planes, respectively. A fairly symmetric and single peak (111) face is shown by XRD profiles of the Au-Pt bimetallic system, which is intermediate of Au and Pt (111) peaks [24,25].

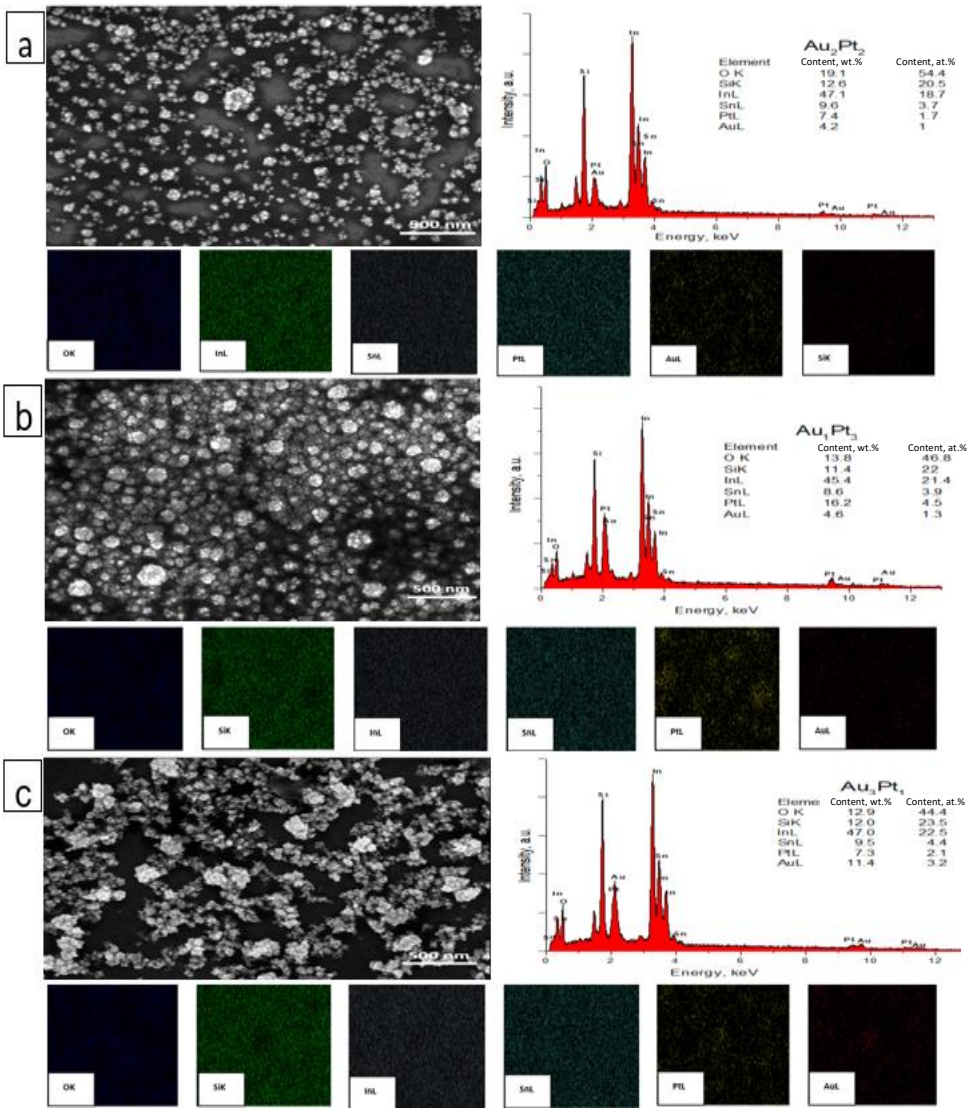

***Figure 3**. FE-SEM, EDX analysis and elemental X-ray mapping of (a) Au_2Pt_2NP/APTES/ITO, (b) Au_1Pt_3NP/APTES/ITO, (c) Au_3Pt_1NP/APTES/ITO electrodes*

Moreover, the values of Au-Pt hybrid nanoparticles lattice constant (*d*) are in between values of monometallic gold (0.407 nm) and platinum (0.392 nm) and increase linearly on increasing mole fraction of platinum in the electrolyte solution. Vegard's law was used to calculate lattice constant (d), which suggests an alloy feature in deposited Au-Pt hybrid where Au and Pt atoms are mixed tightly [28].

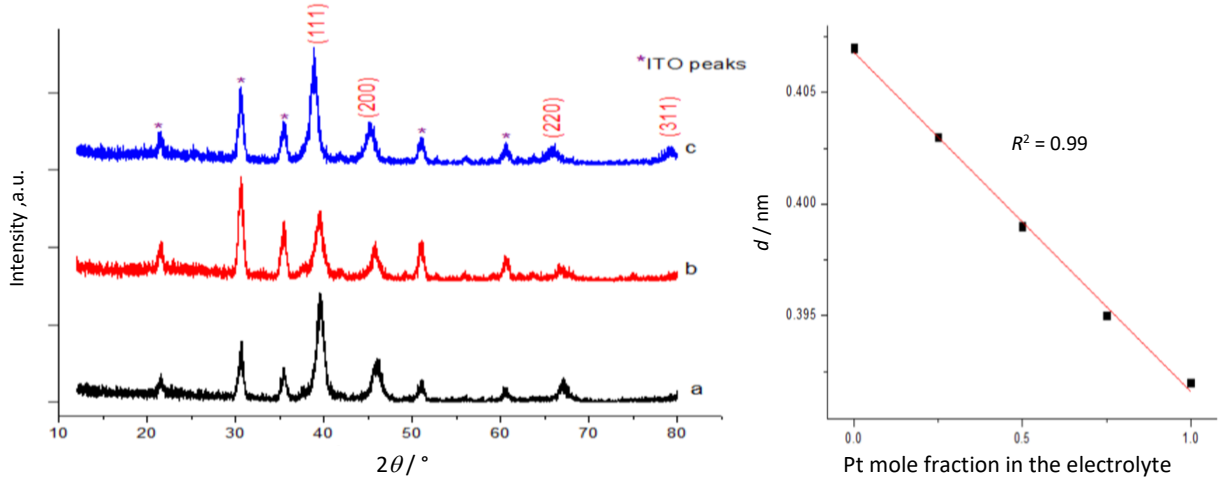

***Figure 4.** (Left) XRD of (a) Au_1Pt_3NP/APTES/ITO, (b) Au_2Pt_2NP/APTES/ITO, (c) Au_3Pt_1NP/APTES/ITO electrodes, and (right) plot for their lattice constant*

***Table 2**. Peak positions and d values for various prepared electrodes*

Electrode type	2θ / °				*d* / nm	Au:Pt part ratio in electrolyte	DB card number
	111	200	220	311			
AuNP/APTES/ITO [25]	38.18	44.36	64.60	77.61	0.407	4:0	00-001-1172
Au_3Pt_1NP/APTES/ITO	38.98	45.42	65.75	79.17	0.403	3:1	00-015-0043
Au_2Pt_2NP/APTES/ITO	39.41	45.74	66.97	-	0.399	2:2	00-015-0043
Au_1Pt_3NP/APTES/ITO	39.67	46.11	66.03	79.56	0.395	1:3	00-015-0043
PtNP/APTES/ITO [24]	39.75	46.33	67.69	-	0.392	0:4	00-001-1194

Absorption spectra analysis of deposited AuPt nanoparticles

UV absorption spectra for AuNP, PtNP and their alloys electrochemically deposited on APTES/ITO electrode surfaces in different ratios were compared in a range of 400 to 800 nm wavelength (Figure 5). No absorption peak was observed for PtNP (Figure 5a), while different broad peaks for AuNP, Au_3Pt_1NP, Au_2Pt_2NP and Au_1Pt_3NP were observed at maximum wavelengths of 567 nm (Figure 5b), 557 nm (Figure 5e), 551 nm (Figure 5c) and 515 nm (Figure 5d), respectively. A left shift of wavelength peaks in the obtained spectrum was observed with the increase of Pt content in the alloy [1].

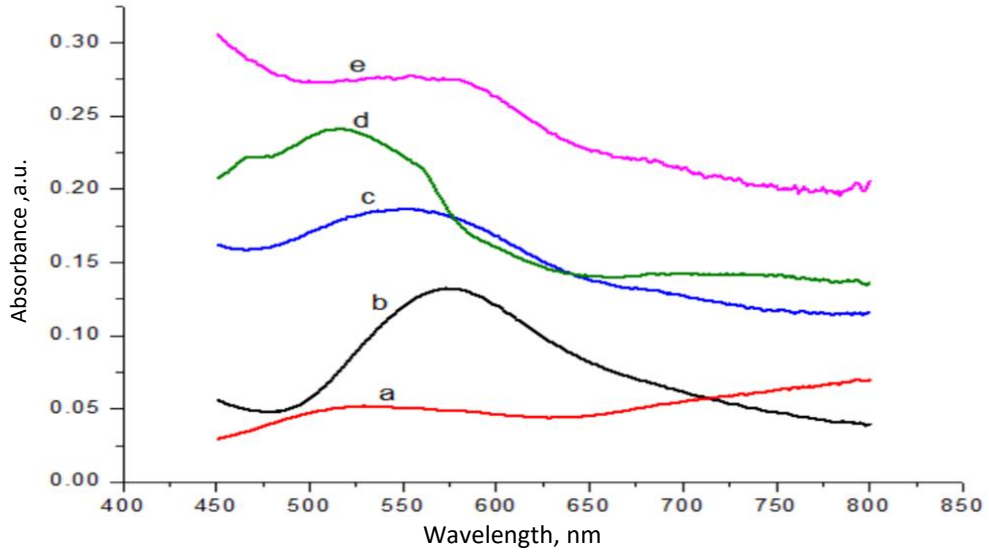

***Figure 5.** UV absorption spectra of: (a) PtNP/APTES/ITO, (b) AuNP/APTES/ITO, (c) Au_2Pt_2NP/APTES/ITO, (d) Au_1Pt_3NP/APTES/ITO, (e) Au_3Pt_1NP/APTES/ITO electrodes*

Electrochemical characterization of different AuPtNP/APTES/ITO-modified electrodes

Further electrochemical investigations were done for all prepared AuPtNP-modified electrodes (Au_3Pt_1NP/APTES/ITO, Au_2Pt_2NP/APTES/ITO and Au_1Pt_3NP/APTES/ITO) in 100 mM PBS buffer solution containing 5 mM of $[Fe(CN)_6]^{3-/4-}$ redox couple. An increase in redox peak currents and a decrease in the separation of peak potential values were observed with the deposition of noble metal alloy nanoparticles on APTES/ITO (Figure 6a), which is reconfirmed by DPV peak current (Figure 6b) and a decrease in resistance of charge transfer (Figure 6c). The corresponding parameters for AuPtNP/APTES/ITO electrodes are summarized in Table 3 and compared with those already obtained for Au and Pt-modified APTES/ITO electrodes [24,25]. Among AuPtNP-modified electrodes, an increase in anodic and cathodic current is maximal for Au_3Pt_1NP/APTES/ITO with ΔI_p 1271.97 µA, for which the lowest charge transfer resistance (R_{ct}) of 319.78 Ω was obtained (Table 3). So, for the preparation of the biosensing electrode, Au_3Pt_1NP/APTES/ITO was used and modified by depositing SAA biomarker-specific antibodies.

***Table 3**. CV redox peak potentials (E_{oxi} and E_{red}), their difference (ΔE_p), peak currents difference (ΔI_p) and charge transfer resistance (R_{ct}) of APTES/ITO modified with metal nanoparticles and their alloys*

Electrode type	E_{oxi} / V	E_{red} / V	ΔE_p / V	ΔI_p / µA	R_{ct} / Ω
AuNP/APTES/ITO [25]	0.27	-0.09	0.36	1029.30	258.65
Au_3Pt_1NP/APTES/ITO	0.30	-0.01	0.31	1271.97	319.78
Au_2Pt_2NP/APTES/ITO	0.25	-0.01	0.27	1102.11	333.88
Au_1Pt_3NP/APTES/ITO	0.26	0.03	0.23	1235.57	407.65
PtNP/APTES/ITO [24]	0.25	0.06	0.19	1130.31	430.68

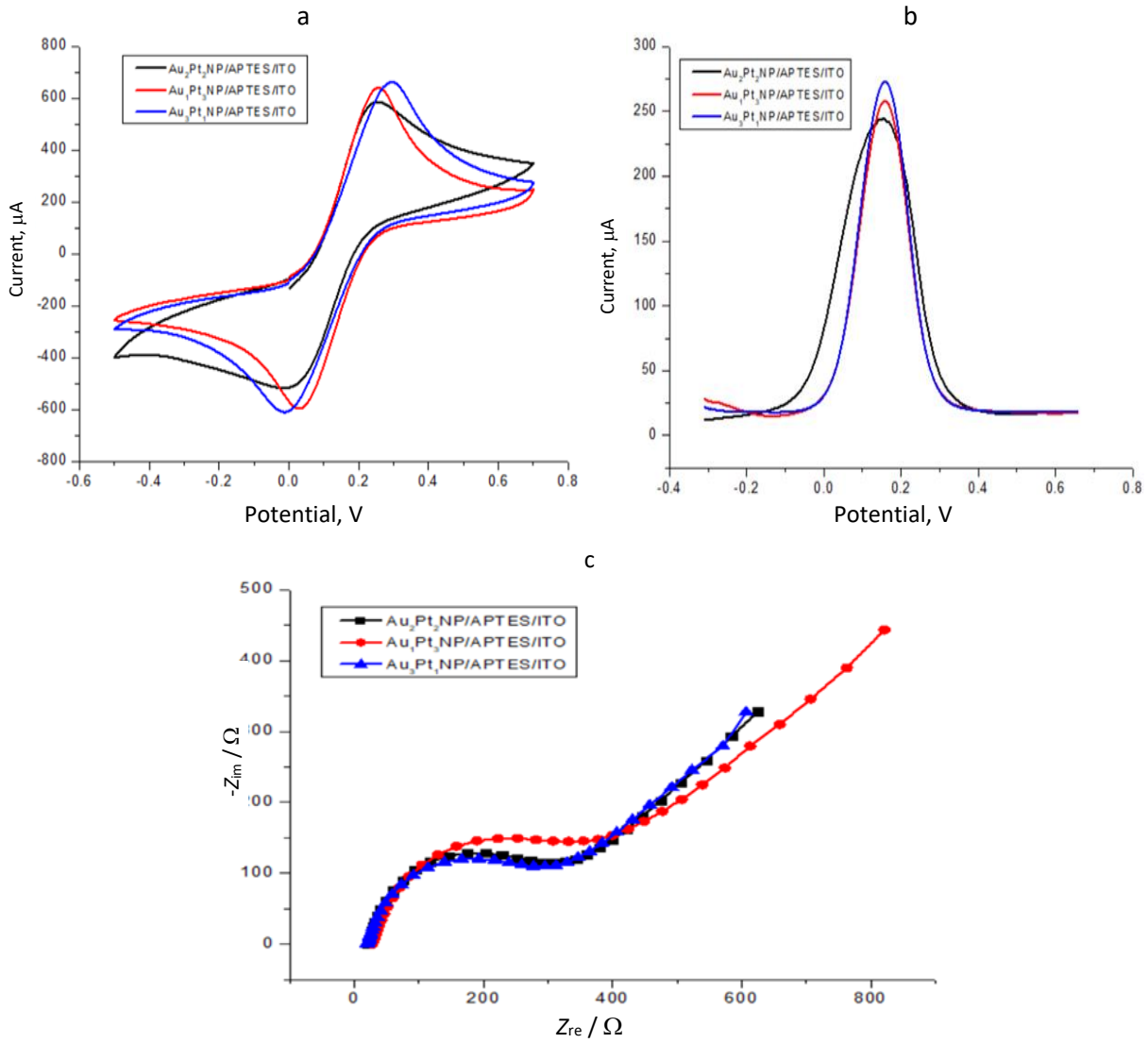

***Figure 6.** (a) CVs at 50 mV s^{-1}, (b) DPVs and (c) EIS at 0.03 V (10^5-0.1 Hz) of different AuPtNP alloys (deposited for 60 cycles from solution A on APTES/ITO in various ratios) in 100 mM PBS, pH 7.4 containing 5 mM $[Fe(CN)_6]^{3-/4-}$*

SAA ½ antibodies immobilization on Au_3Pt_1NP/APTES/ITO

Solution of SAA ½ antibodies of concentration 10 µg ml^{-1} was prepared as reported in our previous work [24,25], and 20 µl were poured on the surface of Au_3Pt_1NP/APTES/ITO electrode and left for the whole day for immobilizing antibodies by self-assembled monolayer (SAM). Such prepared immunoelectrode (SAA-Ab/Au_3Pt_1NP/APTES/ITO) was further used for biosensing of biomarker SAA by various electrochemical techniques [24,25].

Electrochemical properties of SAA-Ab/Au_3Pt_1NP/APTES/ITO electrode

The electrochemical properties of bare Au_3Pt_1NP/APTES/ITO and SAA-Ab/Au_3Pt_1NP/APTES/ITO electrodes in the presence of the $[Fe(CN)_6]^{3-/4-}$ redox couple were defined by different electrochemical techniques, *i.e.* CV, differential pulse voltammetry (DPV) and EIS (Figure 7). The observed variations in peak potential difference (ΔE_p) and peak redox currents (ΔI_p) for recorded CVs profiles in 100 mM PBS buffer solution containing 5 mM $[Fe(CN)_6]^{3-/4-}$ in -0.5 to 0.7 V potential range and at 50 mV/s scan rate, have indicated variations in current values and other parameters, not only between two electrodes, but for ITO and APTES/ITO electrodes [24,25] too. CV of bare ITO showed ΔE_p of 0.27 V, oxidation and reduction peak potentials at 0.26 and -0.02 V, respectively, and ΔI_p of 1078.68 µA [24,25]. Decreased ΔI_p value (775.21 µA) was obtained when ITO was modified with APTES with an increased (ΔE_p) value of 0.59 V. This decrease in ΔI_p value could be due to inhibition in electron transfer between the redox probe and the surface of the electrode, which also confirms the modification with APTES [24,25]. An increased ΔI_p value (1271.97 µA) was seen for Au_3Pt_1NPs modified APTES/ITO electrode with ΔE_p 0.31 V, which can be due to the large surface area and increased conductivity provided by electrochemical deposition of AuPtNPs. This led to faster electron transfer between the redox probe and AuPtNPs modified ITO electrode.

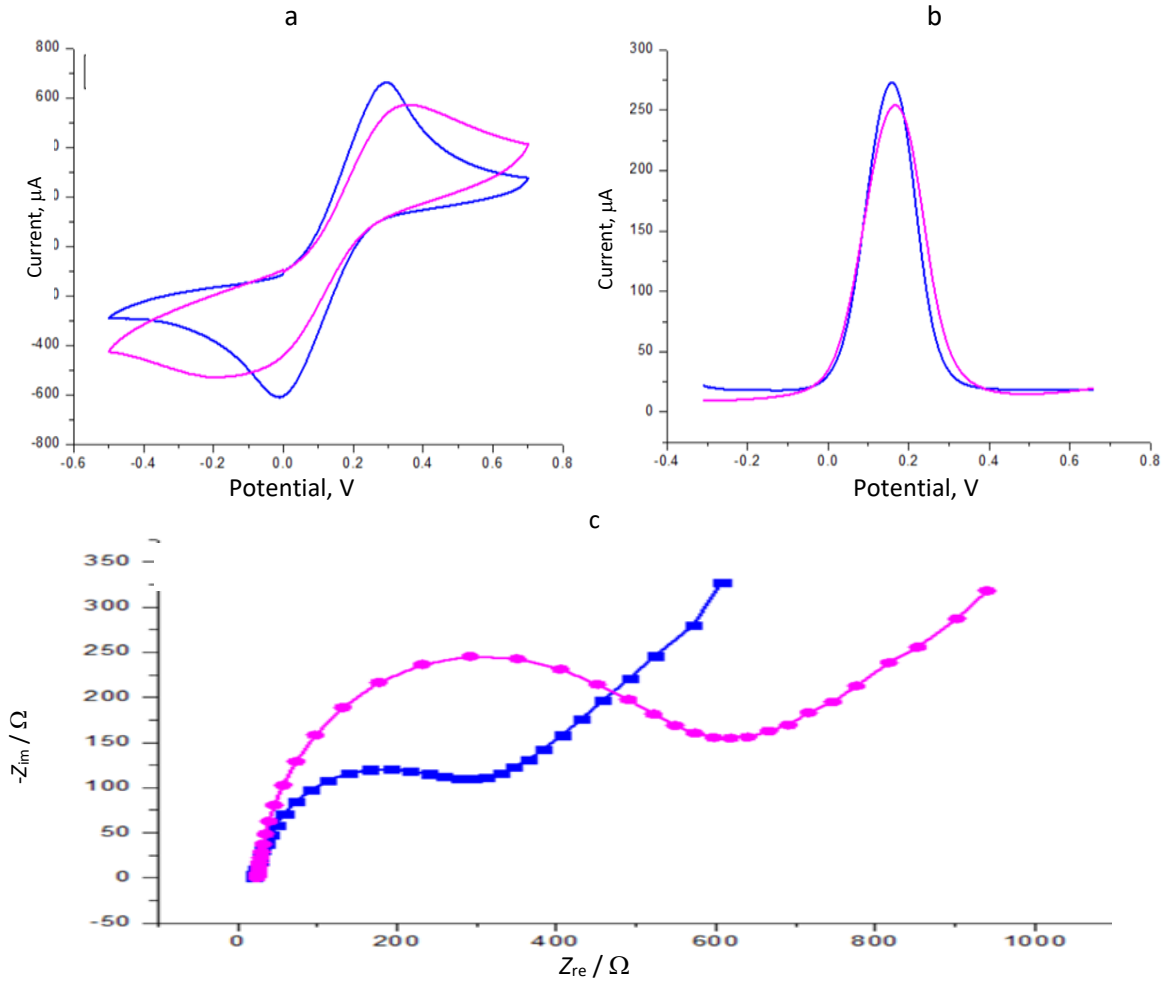

Figure 7. *(a) CV at 50 mV s^{-1}, (b) DPV and (c) EIS at 0.03 V (10^5-0.1 Hz) of ■ Au_3Pt_1NP/APTES/ITO and ● SAA-Ab/Au_3Pt_1NP/APTES/ITO electrodes in 100 mM PBS, pH 7.4 containing 5 mM $[Fe(CN)_6]^{3-/4-}$. Au_3Pt_1NP were deposited for 60 cycles from solution A on APTES/ITO electrode*

Decreased ΔI_p (1100.10 µA) and increased ΔE_p (0.55 V) values were obtained with redox peak potential at -0.20 and 0.36 V, respectively, when the Au_3Pt_1NP/APTES/ITO electrode was modified

with specific antibodies (SAA-Ab/Au_3Pt_1NP/APTES/ITO). This could be ascribed to the insulating layer formation after antibodies immobilization on the electrode surface, which hinders electron transfer between immunoelectrode and redox probe. The pattern of variations obtained for redox peak currents was similar to the pattern of current variations in DPV scans (Figure 7b) of all these modifications of ITO (in -0.3 to 0.7 V potential range) [1,27].

Further, the electrochemical impedance spectroscopy (EIS) technique was used to compare the electrochemical properties of Au_3Pt_1NP/APTES/ITO and SAA-Ab/Au_3Pt_1NP/APTES/ITO electrodes. The Nyquist plots obtained after EIS measurements (Figure 7c) indicated variations in impedance spectra for each modification of ITO [29]. In Nyquist plots, a semicircle diameter represents the electron transfer resistance (R_{ct}), which helps to investigate the interfacial properties of the modified electrode [30,31]. The corresponding R_{ct} values for bare ITO, APTES/ITO [24,25], and two ITO modifications presented in Figure 7c are given in Table 4. It was already shown that bare ITO and APTES/ITO showed R_{ct} values of 677.14 and 1728.64 Ω, respectively [24,25]. However, the smallest R_{ct} value (319.78 Ω) was obtained for APTES/ITO modified with Au3Pt1NPs, indicating excellent conductivity of AuPt alloy nanoparticles. After immobilization of SAA ½ antibodies on the surface of the Au_3Pt_1NP/APTES/ITO electrode, the R_{ct} value was increased (568.77 Ω), which refers to the decreased conductivity of electrode SAA-Ab/Au_3Pt_1NP/APTES/ITO due to the insulating layer formation after antibodies immobilization. These resulted in higher impedance of charge exchange due to the insulation property of protein molecules. Variations in R_{ct} values and obtained impedance spectra with different sizes of semicircle region in Nyquist plots confirm different modifications of ITO and are also in conformity with obtained ΔI_p values of CV measurements (Table 4).

Table 4*. CV oxidation and reduction peak potentials, their difference (ΔE_p), peak current difference (ΔI_p) and charge transfer resistance (R_{ct}) for ITO modifications*

Electrode type	E_{oxi} / V	E_{red} / V	ΔE_p / V	ΔI_p / μA	R_{ct} / Ω
ITO [24,25]	0.26	-0.02	0.27	1078.68	677.14
APTES/ITO [24,25]	0.24	-0.34	0.59	775.21	1728.64
Au_3Pt_1NP/APTES/ITO	0.30	-0.01	0.31	1271.97	319.78
SAA-Ab/Au_3Pt_1NP/APTES/ITO	0.36	-0.20	0.55	1100.10	568.77

Scan rate studies of fabricated electrodes

Scan rate studies were also performed for Au_3Pt_1NP/APTES/ITO and SAA-Ab/Au_3Pt_1NP/APTES/ITO modified electrodes in 100 mM PBS buffer solution containing 5 mM $[Fe(CN)_6]^{3-/4-}$ in the scan rates range of 10 to 200 mV/s (Figure 8). As seen in Figures 8a and c, with every increase in the scan rate, an increase in redox peak current is observed [7]. The ratio of redox peak currents (I_{pc} and I_{pa}) was near one. The quasi-reversible nature of CV and electron transfer kinetics were confirmed by this ratio, which is supported by an increase in peak potential difference, ΔE_p, with an increase in the scan rate. Linear plots of redox peak currents (I_{pa} and I_{pc}) and square root of scan rate (ν) were obtained for all examined modified electrodes in the scan rates range of 10 to 200 mV/s (Figures 8b and 8d).

Electrochemical response to SAA biomarker

A stock solution of concentration 100 μg ml^{-1} of SAA biomarker was prepared as was reported in our previous work [24,25]. DPV technique was used to investigate the electrochemical current in a potential range of -0.3 to 0.7 V. As seen in Figure 9a, the oxidation peak current response of immunoelectrode SAA-Ab/Au_3Pt_1NP/APTES/ITO as a function of concentration of SAA biomarker revealed

linear decrease in recorded DPVs, when 10 µl of SAA biomarker was poured from concentrations range of 10, 10^2, 10^3, 10^4, 10^5 and 10^6 fg ml^{-1}, and kept on the immunoelectrode for 10 minutes every time. The current decrease could be due to the formed SAA/SAA-Ab, which hinders the electron transfer. The linear relationship between DPV peak current values (with negative slope) and the concentration range of the SAA biomarkers can be seen in the obtained calibration plot (Figure 9b) [32]. The linearity is defined by equation (1):

$$I = -24.08703 \log c_{SAA} + 263.91593 \quad (1)$$

The regression coefficient for the linearity equation (R^2) is 0.94. Using equation 3σ/sensitivity (where σ is the standard deviation, which indicates a "typical" deviation from the mean), the limit of detection (LOD) was calculated as 7.0 fg ml^{-1}. The sensitivity of fabricated bioelectrodes was determined by linearity curve slope [33-35].

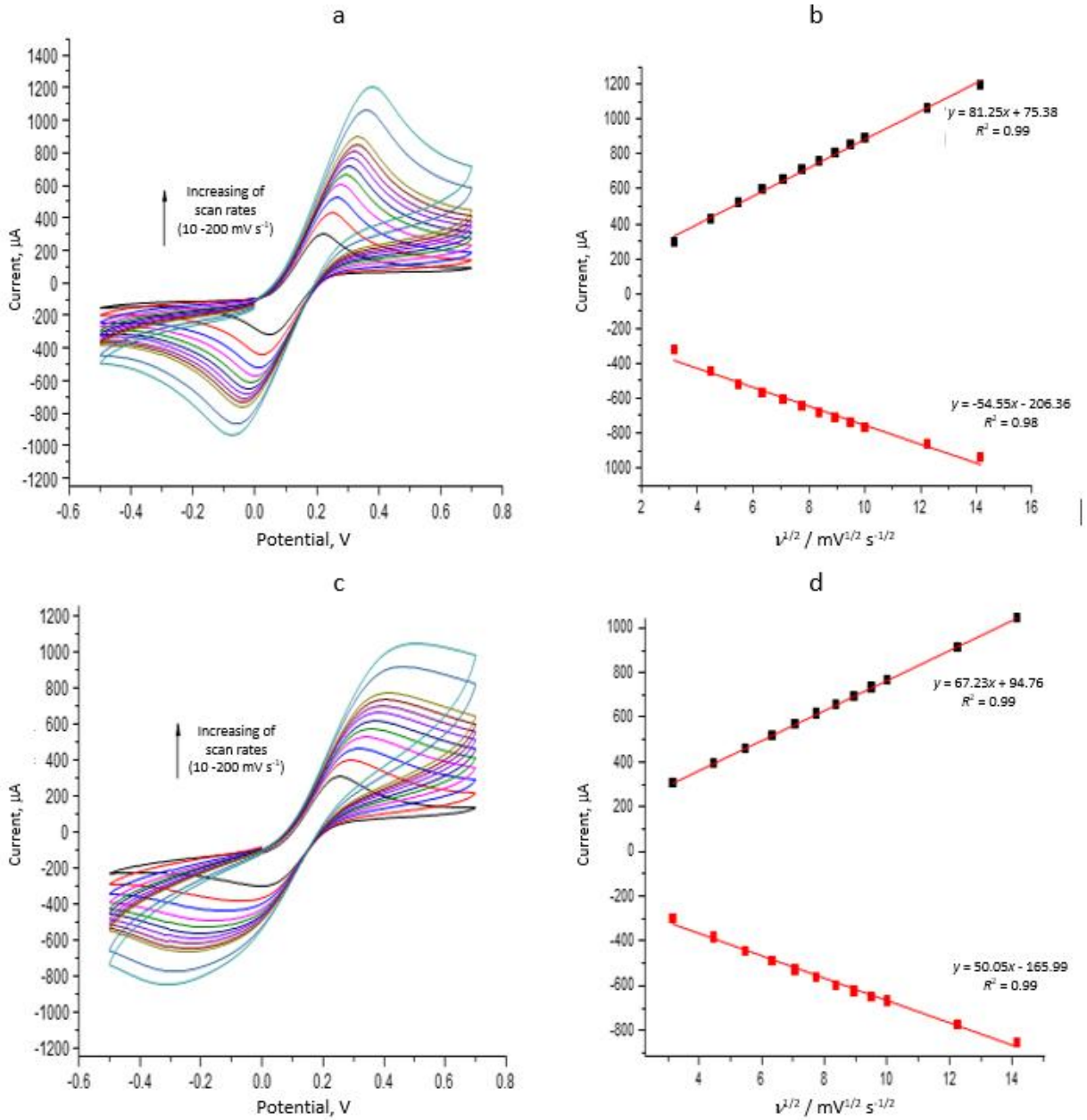

Figure 8. *CV plots at scan rates from 10 mV to 200 mV s^{-1} (left) and linear plots of reduction and oxidation peak currents against square root of scan rate, with indicated linear equations and* R^2 *values (right) of (a) and (b) Au_3Pt_1NP/APTES/ITO; (c) and (d) SAA-Ab/Au_3Pt_1NP/APTES/ITO electrodes in 100 mM PBS containing 5 mM $[Fe(CN)_6]^{3-/4-}$. Au_3Pt_1NP were deposited for 60 cycles from solution A on APTES/ITO electrode*

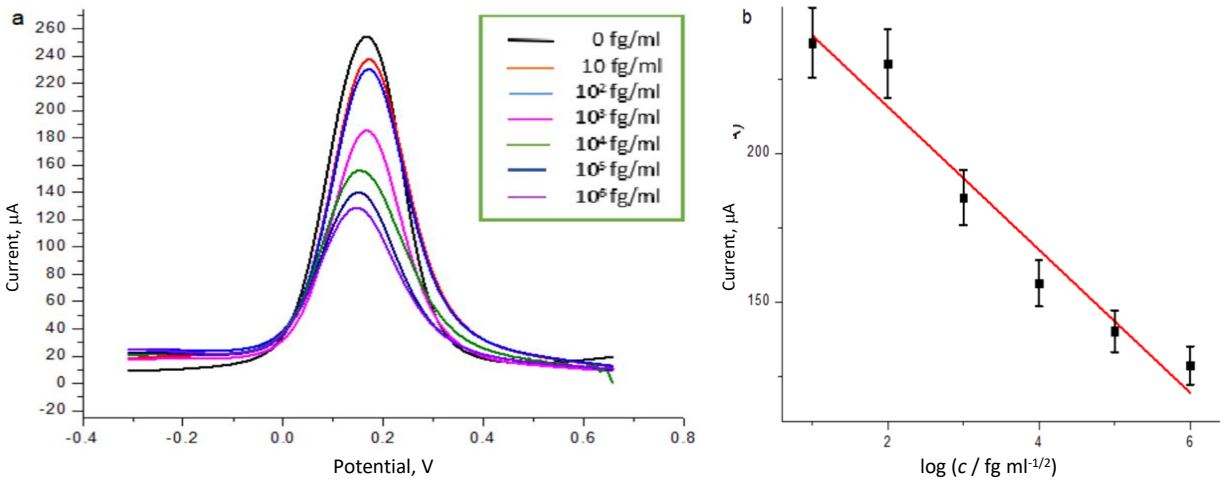

Figure 9. *DPVs (a) and calibration plot (b) for SAA-Ab/Au_3Pt_1NP/APTES/ITO immunoelectrode for SAA biomarker in the concentration range from 10 to 10^6 fg ml^{-1}*

Conclusion

Parameters for electrochemical deposition of AuPt nanoparticles (AuPtNP) alloy from solutions containing different molar fractions of Au and Pt salts on ITO modified by 3-aminopropyltriethoxysilane (APTES) surfaces were optimized. The prepared AuPtNPs/APTES/ITO electrodes, having different part ratios of Au and Pt, were characterized by XRD, FESEM, EDAX and UV absorption techniques, confirming different morphologies and the presence of two metals in various modifications at electrode surfaces. Electrochemical testing of electrodes performed by CV and EIS techniques using a redox probe showed that Au/Pt alloy with the part ratio of 3:1, *i.e.,* Au_3Pt_1NP/APTES/ITO electrode displayed excellent electrocatalytic activity. This electrode was used for SAA-specific antibody immobilization to fabricate the immunoelectrode SAA-Ab/Au_3Pt_1NP/APTES/ITO, successfully detecting SAA biomarkers in the 10 to 106 fg ml^{-1} concentration range. A linear relationship was obtained between increasing SAA concentrations and decreasing peak current values of recorded DPVs, with a calculated LOD of 7.0 fg ml^{-1}.

Conflict of interest*: There* is no conflict of interest as per the authors declaration.

Acknowledgements*:* The authors acknowledge gratefully the support of The NorthCap University & CRF laboratory (Central Research Facility laboratory) for their infrastructure facilities and instrumentation. Authors also thank for financial support received by A. S. Ghrera from Science and Engineering Board (DST), India under Young Scientist research project (YSS/2015/001330).

References

[1] Y. Song, Y. Ma, Y. Wang, J. Di, Y. Tu, Electrochemical deposition of gold-platinum alloy nanoparticles on an indium tin oxide electrode and their electrocatalytic applications, *Electrochimica Acta* **55** (2010) 4909-4914. https://doi.org/10.1016/j.electacta.2010.03.089

[2] F. Xiao, F. Zhao, Y. Zhang, G. Guo, B. Zeng, Ultrasonic Electrodeposition of Gold−Platinum Alloy Nanoparticles on Ionic Liquid−Chitosan Composite Film and Their Application in Fabricating Nonenzyme Hydrogen Peroxide Sensors, *The Journal of Physical Chemistry C* **113** (2009) 849-855. https://doi.org/10.1021/jp808162g

[3] Y. Zhou, G. Yu, F. Chang, B. Hu, C.-J. Zhong, Gold-platinum alloy nanowires as highly sensitive materials for electrochemical detection of hydrogen peroxide, *Analytica Chimica Acta* **757** (2012) 56-62. https://doi.org/10.1016/j.aca.2012.10.036

[4] H. Shen, M. Wang, W. Zhang, Y. Zhang, W. Wang, X. Cao, The bimetallic heterostructure Pt-Au nanoparticle array on Indium Tin Oxide electrode by electrodeposition and their high activity

for the electrochemical oxidation of methanol, *Journal of Alloys and Compounds* **895** (2022) 162581. https://doi.org/10.1016/j.jallcom.2021.162581

[5] A. Kathalingam, K.P. Marimuthu, K. Karuppasamy, Y.-S. Chae, H. Lee, H.-C. Park, H.-S. Kim, Structural and Mechanical Characterization of Platinum Thin Films Prepared Electrochemically on ITO/Glass Substrate, *Metals and Materials International* **27** (2021) 1554-1564. https://doi.org/10.1007/s12540-019-00527-5

[6] H. Yu, J. Yu, L. Li, Y. Zhang, S. Xin, X. Ni, Y. Sun, K. Song, Recent Progress of the Practical Applications of the Platinum Nanoparticle-Based Electrochemistry Biosensors, *Frontiers in Chemistry* **9** (2021) 677876. https://doi.org/10.3389/fchem.2021.677876

[7] R. Chauhan, B. Nagar, P. R. Solanki, T. Basu, Development of Triglyceride Biosensor Based on a Platinum Nano Particle and Polypyrrole Nano Composite Electrode, *Materials Focus* **2** (2013) 316-323. https://doi.org/10.1166/mat.2013.1096

[8] P. Si, N. Razmi, O. Nur, S. Solanki, C. M. Pandey, R. K. Gupta, B. D. Malhotra, M. Willander, A. de la Zerda, Gold nanomaterials for optical biosensing and bioimaging, *Nanoscale Advances* **3** (2021) 2679-2698. https://doi.org/10.1039/D0NA00961J

[9] T. Ahuja, V. K. Tanwar, S. K. Mishra, D. Kumar, A. M. Biradar, A. M. Rajesh, Immobilization of Uricase Enzyme on Self-Assembled Gold Nanoparticles for Application in Uric Acid Biosensor, *Journal of Nanoscience Nanotechnology* **11** (2011) 4692-4701. https://doi.org/10.1166/jnn.2011.4158

[10] H. H. Kyaw, S. H. Al-Harthi, A. Sellai, J. Dutta, Self-organization of gold nanoparticles on silanated surfaces, *Beilstein Journal of Nanotechnology* **6** (2015) 2345-2353. https://doi.org/10.3762/bjnano.6.242

[11] G. Zhao, G. Liu, Electrochemical Deposition of Gold Nanoparticles on Reduced Graphene Oxide by Fast Scan Cyclic Voltammetry for the Sensitive Determination of As(III), *Nanomaterials* **9** (2018) 41. https://doi.org/10.3390/nano9010041

[12] M. Z. H. Khan, Nanoparticles Modified ITO Based Biosensor*, Journal of Electronic Materials* **46** (2017) 2254-2268. https://doi.org/10.1007/s11664-016-5172-3

[13] Md. Z. H. Khan, Effect of ITO surface properties on SAM modification: A review toward biosensor application, *Cogent Engineering* **3** (2016) 1170097. https://doi.org/10.1080/23311916.2016.1170097

[14] G. H. Sack, Serum amyloid A, *Molecular Medicine* **24** (2018) 46. https://doi.org/10.1186/s10020-018-0047-0

[15] H. Miwata, T. Yamada, M. Okada, T. Kudo, H. Kimura, T. Morishima, Serum amyloid A protein in acute viral infections, *Archives of Disease Childhood* **68** (1993) 210-214. https://doi.org/10.1136/adc.68.2.210

[16] E. Malle, F. C. De Beer, Human serum amyloid A (SAA) protein: a prominent acute-phase reactant for clinical practice, *European Journal of Clinical Investigation* **26** (1996) 427-435. https://doi.org/10.1046/j.1365-2362.1996.159291.x

[17] B. Rezaei, N. Irannejad, *Electrochemical detection techniques in biosensor applications*, in *Electrochemical Biosensors,* A. A. Ensafi, Ed., Elsevier Inc., 2019, 11-43. https://doi.org/10.1016/B978-0-12-816491-4.00002-4

[18] K. Y. Goud, K. K. Reddy, A. Khorshed, V. S. Kumar, R. K. Mishra, M. Oraby, A. H. Ibrahim, H. Kim, K. V. Gobi, Electrochemical diagnostics of infectious viral diseases: Trends and challenges, *Biosensors and Bioelectronics* **180** (2021) 113112. https://doi.org/10.1016/j.bios.2021.113112

[19] C. Xia, Y.n Li, G. Yuan, Y. Guo, C. Yu, Immunoassay for serum amyloid A using a glassy carbon electrode modified with carboxy-polypyrrole, multiwalled carbon nanotubes, ionic liquid and chitosan, *Microchimica Acta* **182** (2015) 1395-1402. https://doi.org/10.1007/s00604-015-1465-0

[20] J.-S. Lee, S.-W. Kim, E.-Y. Jang, B.-H. Kang, S.-W. Lee, G. Sai-Anand, S.-H. Lee, D.-H. Kwon, S.-W. Kang, Rapid and Sensitive Detection of Lung Cancer Biomarker Using Nanoporous Biosensor

Based on Localized Surface Plasmon Resonance Coupled with Interferometry, *Journal of Nanomaterials* **2015** (2015) 183438. https://doi.org/10.1155/2015/183438
[21] C. Timucin, O. Gul, O. Kutuk, H. Basaga, antibody array-based immunosensor for detecting cardiovascular disease risk markers, *Journal of Immunoassay and Immunochemistry* **33** (2012) 275-290. https://doi.org/10.1080/15321819.2011.638407
[22] A. L. Pastore, G. Palleschi, L. Silvestri, D. Moschese, S. Ricci, V. Petrozza, A. Carbone, A. Di Carlo, Serum and Urine Biomarkers for Human Renal Cell Carcinoma, *Disease Markers* **2015** (2015) 251403. https://doi.org/10.1155/2015/251403
[23] I. Sorić Hosman, I. Kos, L. Lamot, Serum Amyloid A in Inflammatory Rheumatic Diseases: A Compendious Review of a Renowned Biomarker, *Frontiers in Immunology* **11** (2021) 631299. https://doi.org/10.3389/fimmu.2020.631299
[24] Kalpana, A. S. Ghrera, Electrochemical Investigation of Viral Respiratory Infection Inflammatory Biomarker Serum Amyloid A Protein by Using PtNP Modified Electrode, *Chemistry Select* **8** (2023) e202203532. https://doi.org/10.1002/slct.202203532
[25] Kalpana, A. S. Ghrera, Electrochemical Investigation of Viral Respiratory Infection Inflammatory Biomarker Protein by Using AuNPs Modified Electrode, *Analytical and Bioanalytical Chemistry Research* **10** (2023) 289-300. https://doi.org/10.22036/ABCR.2023.367377.1849
[26] M.-C. Tsai, P.-Y. Chen, Voltammetric study and electrochemical detection of hexavalent chromium at gold nanoparticle-electrodeposited indium tin oxide (ITO) electrodes in acidic media, *Talanta* **76** (2008) 533-539. https://doi.org/10.1016/j.talanta.2008.03.043
[27] N. Tavakkoli, N. Soltani, Z. K. Tabar, M. R. Jalali, Determination of dopamine using the indium tin oxide electrode modified with direct electrodeposition of gold-platinum nanoparticles, *Chemical Papers* **73** (2019) 1377-1388. https://doi.org/10.1007/s11696-019-00690-4
[28] W. Ye, H. Kou, Q. Liu, J. Yan, F. Zhou, C. Wang, Electrochemical deposition of Au-Pt alloy particles with cauliflower-like microstructures for electrocatalytic methanol oxidation, *International Journal of Hydrogen Energy* **37** (2012) 4088-4097. https://doi.org/10.1016/j.ijhydene.2011.11.132
[29] M. A. MacDonald, H. A. Andreas, Method for equivalent circuit determination for electrochemical impedance spectroscopy data of protein adsorption on solid surfaces, *Electrochimica Acta* **129** (2014) 290-299. https://doi.org/10.1016/j.electacta.2014.02.046
[30] A. S. Ghrera, C. M. Pandey, B. D. Malhotra, Multiwalled carbon nanotube modified microfluidic-based biosensor chip for nucleic acid detection, *Sensors and Actuators B: Chemical* **266** (2018) 329-336. https://doi.org/10.1016/j.snb.2018.03.118
[31] A. Sharma, Z. Matharu, G. Sumana, P. R. Solanki, C. G. Kim, B. D. Malhotra, Antibody immobilized cysteamine functionalized-gold nanoparticles for aflatoxin detection, *Thin Solid Films* **519** (2010) 1213-1218. https://doi.org/10.1016/j.tsf.2010.08.071
[32] Y. G. Gupta, Kalpana, A. Sharma Ghrera, Electrochemical studies of lateral flow assay test results for procalcitonin detection, *Journal of Electrochemical Science and Engineering* **12** (2021) 265–274. https://doi.org/10.5599/jese.1127
[33] Y. Gupta, C. M. Pandey, A. S. Ghrera, Reduced Graphene Oxide-Gold Nanoparticle Nanohybrid Modified Cost-Effective Paper-Based Biosensor for Procalcitonin Detection, *ChemistrySelect* **7** (2022) e202202642. https://doi.org/10.1002/slct.202202642
[34] Y. Gupta, C. M. Pandey, A. S. Ghrera, Development of conducting cellulose paper for electrochemical sensing of procalcitonin, *Microchimica Acta* **190** (2023) 32. https://doi.org/10.1007/s00604-022-05596-9
[35] Y. Gupta, A. S. Ghrera, Development of conducting paper-based electrochemical biosensor for procalcitonin detection, *ADMET & DMPK* **11** (2023) 263-275. https://doi.org/10.5599/admet.1575